Mountain, G.S., Miller, K.G., Blum, P., Poag, C.W., and Twichell, D.C. (Eds.), 1996
Proceedings of the Ocean Drilling Program, Scientific Results, Vol. 150

20. SEQUENCE STRATIGRAPHY AND DIAGENESIS OF THE MIOCENE–OLIGOCENE BELOW THE NEW JERSEY CONTINENTAL SLOPE: IMPLICATIONS OF PHYSICAL PROPERTIES AND MINERALOGICAL VARIATIONS[1]

Adam Vecsei[2] and Bryce W. Hoppie[3]

ABSTRACT

We discuss the origin and sequence stratigraphic implications of physical properties and mineralogical variations in the mid-Miocene to upper Oligocene of the New Jersey continental margin at Site 903. The thick, mostly fine-grained, strongly bioturbated, terrigenous and biogenic sediments reveal continuous long-term and cyclic compositional changes as well as abrupt short-term changes.

The most important long-term changes are early compaction and diagenetic precipitation of carbonate concretions, late diagenetic precipitation and dissolution of calcite, dissolution of biogenic silica, and subsequent precipitation of opal-CT and clinoptilolite. Dissolution of biogenic opal appears to be the main cause of generally downhole decreasing wet-bulk density and increasing porosity. Opal-CT cementation strongly increases in the 40 m immediately above the Eocene chalks, and again deeper in the upper–middle Eocene chalks, forming two distinct diagenetic "fronts."

Integration of physical properties and mineralogical variations allows us to recognize 10 distinct intervals. The intervals and their boundaries compare well with the previously devised seismic stratigraphy of this area and its sequences and systems tracts, although some intervals are too thin to be resolved by the available seismic data.

The intervals reflect changes of sediment composition with progressive continental margin progradation. In the upper Oligocene and subordinately in the Miocene, intervals characterized by high density and distinct mineralogy correlate to sediments between thin, laterally continuous reflectors. These intervals are interpreted as distal slope sediments and as lowstand fans deposited laterally or basinward from prograding deltaic wedges, that is, probably in the early lowstand systems tract. Lithological changes associated with progradation caused sediment bulk density to increase and distinctive mineralogic changes which we interpret as late lowstand and highstand systems tracts.

INTRODUCTION

In recent years, high-resolution physical properties records have been recognized as a proxy of sedimentary processes and paleoceanographic change. The types of processes best resolved depend on their respective influence on sedimentation. For example, wet-bulk density records were used as a paleoceanographic proxy in deep-sea carbonates, with physical properties fluctuations interpreted as a function of orbital forcing (Busch, 1991; Mayer, 1991; Mayer et al., 1993).

In continental margin settings such as the New Jersey slope, most sediments consist of detrital grains and microfossils deposited by either gravitative processes (e.g., turbidity currents), or by hemipelagic settling. The temporal and spatial pattern of deposition is greatly influenced by sediment input and accommodation; the latter is in turn a function of relative sea-level and of total (tectonic, sedimentary compaction, and sea-level and sedimentary load) subsidence. These factors control progradation and retrogradation of the continental margin sediment wedge and thus the sequence stratigraphy (Vail et al., 1977; Van Wagoner et al., 1988). In sediment series that do not allow detailed visual lithofacies analysis (e.g., in many fine-grained sediments), the high-resolution physical properties record, obtained from logging or core measurements, can be a powerful tool for sequence stratigraphic interpretation. Physical properties cycles show trends comparable to natural gamma-ray and spontaneous potential well-logs routinely interpreted in terms of sequence stratigraphy (Mitchum et al., 1993), and thus may be used as another tool of sequence stratigraphic investigation.

In Pleistocene to Eocene sediments drilled during Leg 150 on the New Jersey slope, preliminary comparison of the position of offsets in the physical properties curves with the positions of lithostratigraphic boundaries, biostratigraphic hiatuses, and sequence boundaries suggests that the physical properties record may reflect depositional sequences and/or other paleoceanographic factors (Shipboard Scientific Party, 1994a). We investigate the origin and significance of cyclicity in the physical properties of mid-Miocene to upper Oligocene sediments at Site 903 where the thickest sediments of this age were recovered. In order to understand the origin and significance of the cycles, we will explore the mineralogical, microstructural, and diagenetic properties of these siliciclastic and biogenic sediments by mineralogical and chemical analysis, and by microscopy.

GEOLOGICAL SETTING

The Neogene section of the "Baltimore Canyon Trough" off New Jersey (Fig. 1) is thick, stratigraphically relatively complete, and was deposited in a simple and largely undisturbed rifted-margin tectonic setting. Industry and academia have explored these sediments with a dense grid of seismic surveys, drilling, and outcrop study of equivalent onshore sequences (e.g., Schlee, 1981; Mountain and Tucholke, 1985; Poag, 1985, 1987; Schlee and Hinz, 1987; Miller et al., 1990). Thus, studies of the sequence stratigraphy of the sediments below the New Jersey Margin can be based on a large litho-, bio-, and chronostratigraphic data set (e.g., Greenlee and Moore, 1988; Greenlee et al., 1988; Christie-Blick et al., 1990; Greenlee et al., 1992).

The Eocene sediments of the New Jersey Margin are marly nannofossil chalks with common diatoms and radiolarians. The abundance of nannofossils in the North Atlantic Eocene was attributed to

[1]Mountain, G.S., Miller, K.G., Blum, P., Poag, C.W., and Twichell, D.C. (Eds.), 1996. *Proc. ODP, Sci. Results,* 150: College Station, TX (Ocean Drilling Program).

[2]Geologisches Institut der Universität, Albertstrasse 23B, D-79104 Freiburg i.Br., Federal Republic of Germany. adam@perm.geologie.uni-freiburg.de

[3]Earth Sciences Department, University of California, Santa Cruz, Santa Cruz, CA 95064, U.S.A.

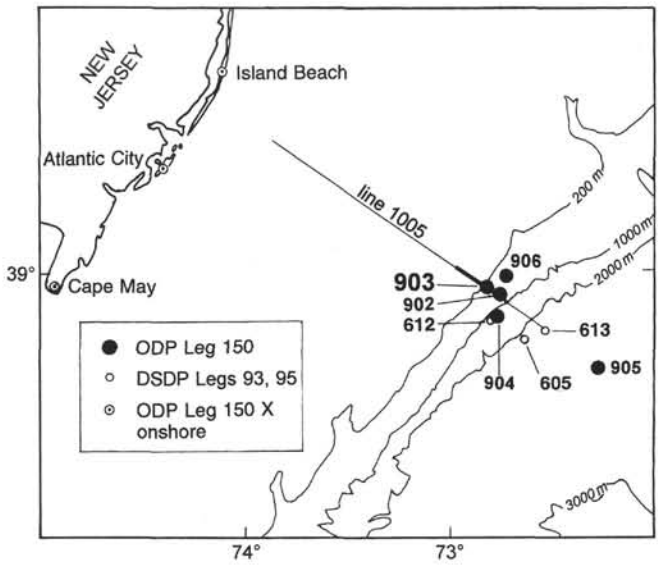

Figure 1. Site 903 and other drill sites of the New Jersey continental margin transect. Bold part of the trace of seismic section Ew9009 Line 1005 indicates the segment interpreted in Figure 9.

the shelf-ocean fractionation of carbonate as a function of long-term sea-level change (Thiede, 1981), and to high fertility of siliceous organisms resulting from the circulation pattern in the evolving Atlantic (Ramsay, 1973). The Oligocene to Quaternary is characterized by mostly fine-grained terrigenous sediments with varying amounts of biogenic components (mainly diatoms). The causes of increased terrigenous input during the Neogene are still disputed, but accelerated tectonic uplift and denudation of the Appalachian hinterland was probably the main factor (cf. Hack, 1982). The intermittent abundance of siliceous organisms during the Neogene is related to the periodic intensification of currents that brought nutrient-rich waters from the cool Arctic region (Riech and von Rad, 1979).

A second-order sea-level rise caused landward retrogradation and subsequent aggradation of the upper Oligocene and lower Miocene sequences on the New Jersey Margin (Greenlee and Moore, 1988); a contrasting interpretation involves auto-cyclicity (Steckler et al., 1993). The sequences prograded considerably during the subsequent middle and late Miocene sea-level highstand and fall. As a consequence of this geometry, Site 903 drilled the Oligocene and lower Miocene sequences in their thin distal parts far seaward of the paleoshelf edge, whereas sequences of middle to late Miocene age were penetrated in their thicker segments slightly seaward of the paleoshelf edge (Miller and Mountain, 1994). These sediments are mainly muds and mudstones; coarse and commonly glauconitic sands are usually restricted to the base of the sequences. Rare slumps occur. The types of depositional processes that caused these lithologies are as yet largely unknown, as pervasive bioturbation destroyed most primary sedimentary structures. Previous studies in this area characterize the depositional setting as prograding deltas and intervening continental slope or rise areas (cf. Poag, 1987; McMaster et al., 1989; Steckler et al., 1993).

METHODS AND INTERPRETATION PROCEDURES

Physical Properties

Wet-bulk density is a function of both porosity (the pores being filled by water and/or gas) and grain (i.e., dry-bulk) density. Several factors may contribute to wet-bulk density variations. Mineral density is the dominant factor in sediments composed predominantly of isometric grains (see below); interparticle pores tend to be small in such sediments. Wet-bulk density is also controlled by the presence of large interparticle pores between nonaligned platy minerals (e.g., clays and micas), and large intraparticle pores in the frustules and tests of biogenic particles (mainly diatoms, radiolarians, and foraminifers at Site 903), and in molds of dissolved fossils.

Table 1. Densities of minerals and organic components common in Site 903 sediments.

Mineral (group)	Density (g/cm^3)
Glauconite	2.3–2.54
Illite	2.66
Kaolinite	2.59
Calcite	2.71
Feldspars (orthoclase, anorthite)	2.57–2.76
Opal-A	1.7–2.05
Terrestrial plant material	1.0–1.5
Dolomite	2.89
Siderite	3.94
Pyrite	5.01

Note: From Olhoeft and Johnson (1989), except opal-A from Hurd and Theyer (1977) and terrestrial plant material from Robert (1985).

A nearly continuous (i.e., 2–2.5 cm sample spacing) approximation of wet-bulk density was obtained by an automated gamma-ray attenuation porosity evaluator (GRAPE; Shipboard Scientific Party, 1994a). The GRAPE calculates wet-bulk density using the gamma-ray attenuation coefficient of quartz (Boyce, 1973, 1976); the gamma-ray attenuation coefficients of the other common sedimentary minerals differ little from that of quartz, so that the significantly lower attenuation coefficient of water and gas in the pores mainly control the calculated density. Successive GRAPE wet-bulk densities from the same core sections scatter considerably toward low values. This may be due to coring disturbances. We consider only the highest of adjacent GRAPE values, which can be assumed to represent undisturbed sediment. These high values usually show the same trends and are similar, although partly lower than those of wet-bulk density gravimetrically measured in discrete core samples. Systematic offsets between gravimetric and GRAPE densities are discussed and corrected by Hoppie (this volume). Because of poor core recovery and quality, GRAPE data obtained in Hole 903C sediments between 770 and 1050 meters below sea floor (mbsf) will not be used for interpretation. Note that GRAPE wet-bulk density significantly deviates from gravimetrically measured wet-bulk density in discrete samples in two intervals at Site 903 (see below), indicating some sampling inconsistencies.

The gravimetric wet-bulk density, grain density, and porosity were determined on board the *Resolution* in discrete samples taken at regularly spaced intervals and from representative minor lithologies (Shipboard Scientific Party, 1994a). Grain density is a function of mineral densities (Table 1). The low mineral densities of opal-A (in diatoms and radiolarians, which constitute a major portion of many sediments at Site 903) and of terrestrial plant material (present at Site 903 in minor but variable amounts) cause lower grain density. In early diagenetic carbonate concretions, high wet-bulk and grain densities result from a dense matrix that causes low porosity, and from the high mineral density of the carbonates.

Faulty assumptions of gas properties during the pycnometer wet-volume calculation (cf. Nobes et al., 1992) probably caused small systematic offsets in the absolute values of most gravimetrically determined properties. Despite this probable error, the good match of discrete and downhole logging wet-bulk densities indicates the reliability of the gravimetric values (Hoppie, this volume). The systematic errors in the physical properties data were only partly recognized

on board, and they are not corrected in this study because they do not impair our arguments.

Microstructural Analysis

Microstructural analyses of 114 freeze-dried samples were performed by scanning electron microscopic (SEM) observation. Individual minerals were recognized by electron-dispersive X-ray analysis (EDX) attached to the SEM. Microstructural analysis yields qualitative data on detrital and cement minerals and particle orientations (sediment fabric; cf. methods adopted by O'Brien [1987] and Bennett et al. [1991]).

Element and Mineral Composition

The depth distribution of elements and minerals at Site 903, cross-correlation between elements and minerals, and cross-correlation between elements permit normative approximation of some mineral contents and highlight the complex distribution of others. Elemental analysis was performed by X-ray fluorescence (XRF) in 64 fused samples from representative and some minor lithologies (Table 2); analytical error is ±0.25%–0.5% for most elements. Mineral composition was determined by X-ray diffractometry (XRD) in 24 of these samples (Fig. 2; Table 2). The XRD procedures are detailed by Hoppie (this volume); analytical error is estimated at 11%–16%.

Comparison of the depth variations in the silica/aluminum (measured as SiO_2/Al_2O_3) ratio with those of quartz, opal-A, and opal-CT indicates that the main trends in Si abundance are caused by changes in opal-A and quartz content, except in the upper Oligocene where opal-CT is also abundant (Fig. 3). It is obvious from the bulk mineralogy (Fig. 2) that clay minerals (mainly illite, illite/smectite, and kaolinite), glauconite, and feldspars contain most of the Al. The excellent correlation of Al_2O_3 with potassium (K_2O) and titanium (TiO_2) in most samples suggests that most Al is associated with the clay minerals. However, Al_2O_3 shows relatively poor cross-correlations, in decreasing order, with clay minerals, quartz, and feldspars (Fig. 4A), and among the clay minerals it is reasonably correlated only with kaolinite (Fig. 4B). These results suggest that the Al distribution pattern is complex in detail.

Ti shows a characteristic depth distribution with intervals of high Ti/Al ratio; these correlate with peaks in either quartz, illite, and/or illite/smectite (IS) content (Fig. 3). Indeed, TiO_2 cross-correlates well to quartz, but correlates poorly to total clays and feldspars (Fig. 4C). The correlation of TiO_2 to kaolinite, illite/smectite, and illite is similar to that of Al_2O_3; the correlation with kaolinite is the best despite the fact that illite is generally richer in Ti (Rösler, 1981). Because there is a strong TiO_2/Al_2O_3 correlation in all samples (Fig. 4D), several minerals (or mineral groups) must carry Ti; however, Ti is probably associated with (although not necessarily contained within) the Al-rich minerals. We cannot unequivocally identify the Ti-bearing minerals responsible for the good correlation to quartz, although this relationship does identify intervals where non-clay terrigenous minerals are abundant. The excellent Al/Ti correlation also indicates that Al was not significantly scavenged from seawater by adsorption to siliceous fossils, as shown for low-latitude Pacific biogenic silica-rich sediments by Murray et al. (1993).

Potassium (K_2O) is strongly cross-correlated to Al_2O_3 and Fe_2O_3 in many samples (Fig. 5A, B), and these ratios probably represent the average clay composition. A group of samples with distinctly higher K_2O/Al_2O_3 ratios also show high and covarying Fe_2O_3 values. We interpret the latter samples as possessing abundant glauconite, a mineral with variable composition characterized by high concentrations of K and Fe (Hathaway, 1979). This interpretation is largely corroborated by the depth distribution of glauconite determined by XRD and smear-slide analyses (Shipboard Scientific Party, 1994c). Glauconite is both redeposited and authigenic at Site 903 (McCracken et al., this volume) and shows a depth distribution that partly differs from Si and Ti (Fig. 3).

GENERAL TRENDS IN THE PHYSICAL PROPERTIES AND THEIR CAUSES

A complex Milankovitch-type cyclicity in the Quaternary to upper/mid-Miocene sediments at Site 903 contrasts with thick cycles of more or less linear downcore variation in the early/mid-Miocene to upper Oligocene (Shipboard Scientific Party, 1994c). The change occurs around a sedimentary unit comprising thick slumps and sands in the lower part of lithologic Subunit IVA (dated in Zones N10–N12 and the early part of Zone DN8, and correlated to sediments above Reflector m1 [= tuscan of Greenlee et al., 1992] to Reflector m1.5 [= orange]). Although glacially dominated climates (the "ice house world") are thought to have prevailed since the Oligocene, cooling significantly intensified in the mid-Miocene, resulting in widespread Antarctic glaciation (Miller et al., 1991; Frakes et al., 1992). The change in physical properties cycle types suggests that other influences on sedimentation became important on the New Jersey Margin since the mid-Miocene. The processes that conveyed the climatic signal to the sediments are as yet largely unknown.

The physical properties in the mid-Miocene through Oligocene sediments at Site 903 show clear first-order trends. Gravimetric wet-bulk density increases downhole from 1.7 to 2.0 g/cm^3 from 0 to 340 mbsf (Quaternary–lower Pleistocene), remains high (~2.1 g/cm^3) from 340 to 610 mbsf (lower Pleistocene to mid-Miocene), decreases to 1.6 g/cm^3 at 970 mbsf (mid-lower Miocene), and varies around 1.7 g/cm^3 from 970 to 1050 mbsf (lower Miocene–upper Oligocene; Fig. 3; Shipboard Scientific Party, 1994c). The general trends of downhole decreasing wet-bulk and grain densities correlate to compositional changes (Fig. 3), indicating these mineralogical changes are probably the cause.

Wet-bulk densities decrease downhole between 610 and 970 mbsf. This trend is opposite to the typical trend in fine-grained siliciclastic sediments that results from mechanical compaction and chemical porosity reduction (cf. Hamilton, 1976). The range of wet bulk densities (~1.5–2.2 g/cm^3) recorded at these depths is in excess of what can be explained by variations in the density of the common minerals (cf. Fig. 2). In the next sections, we investigate the processes that caused these trends. Note that measurements of physical properties influenced by early diagenetic carbonate nodules, bands, and beds in parts of the Miocene and Oligocene (Hicks et al., this volume) are not considered in the trend analysis.

Clay Fabric

Individual clay minerals together with a downhole increasing number of coccoliths constitute the majority of the matrix. SEM analyses usually show preferential alignment of these clays parallel to bedding (Fig. 6A, B). Such fabric appears to have originated from a random grain arrangement: Individual minerals and aggregates are rotated and obtain a preferred orientation parallel to bedding under the influence of mechanical compaction (Bennett et al., 1991). Random orientation is usually caused by bioturbation (cf. O'Brien, 1987). In uncompacted muds, the bioturbated fabric built by randomly arranged individual grains can be distinguished from a nonbioturbated "cardhouse" structure, in which domains of several grains are randomly arranged, and from parallel fabrics that originate from strong particle alignment by bottom currents (Bennett et al., 1991) or anoxic conditions (Moon and Hurst, 1984).

Dissolution and Precipitation of Calcite

No biogenic or diagenetic calcite was found in the matrix of the mid-Miocene samples (700–750 mbsf). Dissolution of calcium carbonate is almost complete, but the former presence of calcareous nannoplankton is indicated by its preservation in early diagenetic carbonate concretions. The dissolution of calcium carbonate is a result of low pH caused by organic matter degradation (Hicks et al., this vol-

Table 2. XRF and XRD data for sediments from Holes 903A and 903C (Miocene–Oligocene).

Core, section, interval (cm)	Depth (mbsf)	Si	Ti	Al	Fe	Mn	Mg	Ca	Na	K	Carbonates	Quartz	Feldspars	Illite	Illite/ smectite	Kaolinite	Glauconite	Opal-A	Opal-CT
150-903A-																			
49X-3, 83–85	436.83	59.24	0.91	18.45	6.01	0.02	1.54	0.53	1.25	2.74									
49X-6, 82–84	441.32	60.85	0.35	6.64	17.14	0.01	2.24	0.40	0.82	4.58									
55X-1, 68–70	491.58	62.16	0.72	10.74	9.78	0.02	1.58	0.23	1.1	3.17									
55X-3, 82–84	494.72	60.66	0.90	16.16	5.70	0.03	1.39	0.29	1.28	2.46									
60X-1, 64–65	539.84	59.67	0.89	17.69	5.61	0.03	1.50	0.45	1.28	2.82									
65X-1, 113–115	588.23	55.87	0.91	19.70	6.46	0.03	1.67	0.51	1.48	2.90									
69X-5, 17–19	631.77	57.75	0.49	7.87	9.20	0.01	2.17	5.34	1.31	3.28									
70X-2, 24–26	636.94	43.51	0.71	14.59	10.89	0.02	1.22	0.50	0.93	2.02									
72X-5, 75–77	661.15	60.75	0.74	14.80	5.06	0.02	1.31	1.13	1.53	2.00									
74X-3, 99–101	677.79	59.67	0.83	16.86	5.29	0.03	1.37	0.72	1.36	2.09									
75X-3, 80–82	687.30	55.43	0.81	17.20	5.26	0.02	1.39	0.78	1.53	1.88	4	20	8	20	9	20	0	15	0
76X-3, 68–70	696.78	60.05	0.74	16.47	4.86	0.02	1.37	0.89	1.56	2.20									
150-903C-																			
12R-5, 93–94	695.53	60.47	0.74	15.76	4.93	0.02	1.33	0.71	1.71	2.18	6	17	7	6	13	15	16	18	0
13R-3, 30–32	701.50	57.66	0.87	19.17	5.25	0.02	1.34	0.68	1.63	2.35	4	14	7	3	8	23	21	10	0
14R-5, 69–71	714.49	49.07	0.80	18.30	11.33	0.04	2.02	1.17	1.18	1.79									
15R-2, 114–116	719.84	46.93	0.67	14.88	14.19	0.05	2.14	1.56	1.32	1.78									
19R-1, 80–82	757.00	57.67	0.90	21.35	4.02	0.01	1.45	0.50	1.30	2.60	3	18	8	8	19	11	19	12	0
20R-4, 87–89	769.98	58.95	0.76	16.35	5.10	0.02	1.53	1.31	1.62	2.12									
21R-3, 70–72	778.78	61.38	0.76	15.48	4.84	0.02	1.59	0.69	1.49	2.11	4	15	7	8	19	11	17	14	0
23R-3, 70–72	798.60	59.17	0.61	13.68	4.81	0.01	1.33	2.91	1.66	1.85	14	15	7	10	3	8	3	22	0
24R-1, 75–77	804.85	55.85	0.61	12.14	6.66	0.02	1.89	3.77	1.40	2.60									
25R-1, 78–80	814.58	61.42	0.58	11.94	7.48	0.01	1.78	0.43	1.64	2.51	6	22	4	8	10	9	9	20	0
27R-1, 68–69	833.78	58.20	0.58	12.83	5.86	0.01	1.59	1.63	1.73	2.09									
28R-3, 32–34	846.02	60.46	0.46	8.89	5.85	0.00	1.33	2.58	1.59	1.95	8	14	7	9	16	12	15	14	0
29R-1, 78–79	853.18	56.08	0.36	7.30	3.14	0.00	1.01	5.46	1.89	1.20									
29R-6, 27–29	860.17	19.51	0.24	5.68	5.14	0.04	11.24	21.60	0.37	0.79									
31R-1, 74–76	872.44	63.81	0.35	7.30	2.62	0.00	0.74	4.43	2.44	1.00	18	5	8	16	9	7	7	26	0
31R-2, 11–13	873.31	59.31	0.45	7.07	6.87	0.00	1.44	4.73	2.01	1.85	14	7	6	12	18	8	16	14	0
32R-1, 68–70	882.08	58.40	0.48	7.92	3.28	0.00	0.90	4.76	1.86	1.22									
32R-3, 32–33	884.72	55.30	0.31	6.17	9.69	0.00	2.26	4.19	1.87	2.86	20	7	7	16	15	5	4	20	0
33R-5, 81–82	897.91	57.70	0.36	6.54	2.72	0.00	0.86	6.59	2.05	0.99	23	12	8	18	5	7	2	23	0
34R-1, 67–68	901.37	55.72	0.34	8.55	3.16	0.00	1.18	7.52	1.97	1.12									
35R-4, 84–86	914.65	58.38	0.42	8.52	2.96	0.00	1.15	6.99	2.01	1.35	23	8	8	10	13	8	8	19	0
36R-2, 80–82	922.30	54.21	0.32	7.38	2.71	0.00	0.87	9.84	2.35	1.00	30	4	6	9	9	8	5	24	0
37R-3, 70–72	933.40	9.74	0.09	1.81	1.73	0.02	15.01	26.49	0.20	0.29									
38R-3, 82–82	942.47	63.70	0.48	8.36	3.20	0.00	1.06	4.51	1.87	1.42	16	15	6	12	11	6	12	19	0
39R-3, 81–83	952.41	48.31	0.40	8.64	3.01	0.00	1.40	13.49	1.58	1.20									
40R-3, 82–85	962.02	57.96	0.49	10.73	3.80	0.00	1.17	5.03	2.18	1.44									
41R-3, 77–79	971.27	57.99	0.45	9.93	3.78	0.00	1.27	6.20	1.69	1.39	18	7	7	10	20	9	1	16	0
44R-1, 131–133	997.81	16.96	0.19	4.06	3.91	0.04	10.81	26.12	0.40	0.57	88	4	0	0	2	3	0	3	0
44R-2, 30–32	998.30	34.94	0.34	7.26	2.76	0.00	1.36	20.35	1.36	1.04									
45R-1, 73–75	1006.93	10.55	0.11	2.09	3.69	0.02	14.20	28.31	0.22	0.62									
45R-2, 76–78	1008.46	54.18	0.52	9.83	4.19	0.01	1.45	9.94	1.24	1.64	25	16	9	3	14	8	7	18	0
46R-1, 10–12	1015.90	57.22	0.39	6.35	0.501	0.00	1.29	11.36	1.13	1.92									
47R-1, 57–58	1026.07	57.61	0.47	7.42	8.25	0.01	1.75	6.73	1.13	2.98	19	18	6				14	15	0
47R-2, 67–68	1027.67	59.64	0.67	10.70	5.29	0.01	1.62	5.65	1.26	2.12	10	19	7	5	17	5	19	15	0
48R-2, 75–77	1031.35	57.82	0.47	7.16	5.76	0.01	1.38	9.35	1.10	2.21									
49R-2, 73–75	1036.02	55.51	0.47	7.41	5.35	0.01	1.39	10.17	1.16	2.03	28	21	7	0	9	1	4	18	13
51R-4, 74–76	1058.36	61.07	0.34	6.86	3.46	0.00	1.10	9.35	1.19	1.33	22	6	5	10	9	7	0	8	31
51R-6, 74–77	1061.36	56.24	0.33	6.95	4.00	0.00	1.15	11.02	1.16	1.55	28	11	5	3	5	1	0	9	35
51R-7, 46–48	1062.58	60.48	0.23	5.12	11.79	0.00	2.15	5.02	0.86	3.34									
51R-7, 125–127	1063.37	69.08	0.18	4.48	10.55	0.00	2.01	1.69	0.78	3.28	10	6	0	0	5	1	12	11	49
51R-8, 44–47	1064.06	40.57	0.38	9.02	8.06	0.00	2.03	15.46	1.03	2.51									
52R-1, 9–12	1064.19	14.23	0.16	4.33	6.43	0.03	8.44	29.10	0.46	0.63									
52R-1, 29–32	1064.39	15.81	0.15	3.99	4.46	0.02	6.47	31.93	0.48	0.55									
52R-1, 67–70	1064.77	34.19	0.26	6.68	3.12	0.01	3.56	23.95	0.87	0.92									
52R-4, 72–74	1069.32	41.15	0.26	7.07	1.95	0.00	1.31	23.41	1.09	0.93									
55R-3, 57–58	1096.37	37.93	0.32	7.80	2.41	0.00	1.30	24.03	1.10	0.97									
56R-3, 44–45	1105.12	47.11	0.32	8.20	2.56	0.00	1.48	19.19	1.17	0.96									
56R-6, 44–47	1109.62	36.37	0.28	7.23	2.15	0.00	1.26	25.90	1.03	0.91									
56R-6, 67–70	1109.85	31.56	0.27	6.78	2.27	0.01	1.15	28.36	0.99	0.88									
57R-2, 49–50	1113.49	36.22	0.34	8.04	2.17	0.00	1.32	25.17	1.00	1.13									
57R-4, 89–90	1116.89	29.74	0.23	5.44	1.72	0.01	1.05	31.66	0.81	0.66									
58R-7, 78–80	1129.54	27.35	0.08	2.45	1.01	0.01	0.63	35.86	0.63	0.40									
58R-8, 24–26	1130.50	36.27	0.22	6.48	1.91	0.01	1.18	25.76	0.93	0.85									

Note: Element analyses in weight percent; minerals (groups) in %XRD counts (see "Methods and Interpretation Procedures" section, this chapter) for details.

ume). Calcareous nannoplankton dissolution contributed to the generation of small pores, decreasing wet-bulk density and increasing porosity downhole. The abundance of calcareous nannoplankton and small calcite cements significantly increases above the Eocene chalk (900–1150 mbsf; Fig. 7B).

Dissolution of Opal-A

Diatoms frustules and, less commonly, radiolarians become abundant from the upper Miocene downward. They are common in the mid-Miocene, but the number of preserved fossils decreases downhole to the upper Oligocene (800–1150 mbsf). This downhole decrease appears to be primarily due to increasing dissolution of biogenic opal-A because SEM imaging shows a concomitant increase in the number of diatom-shaped pores outlined by the compacted fine-grained matrix of the sediments (Fig. 7A). The large number of these pores indicates that mechanical compaction was largely completed before the siliceous fossils dissolved. The depth interval of siliceous tests dissolution corresponds to sediments in which downhole decreasing wet-bulk density and increasing porosity were measured, indicating that these parameters are genetically linked. The siliceous fossils are partly preserved in the upper Eocene chalk.

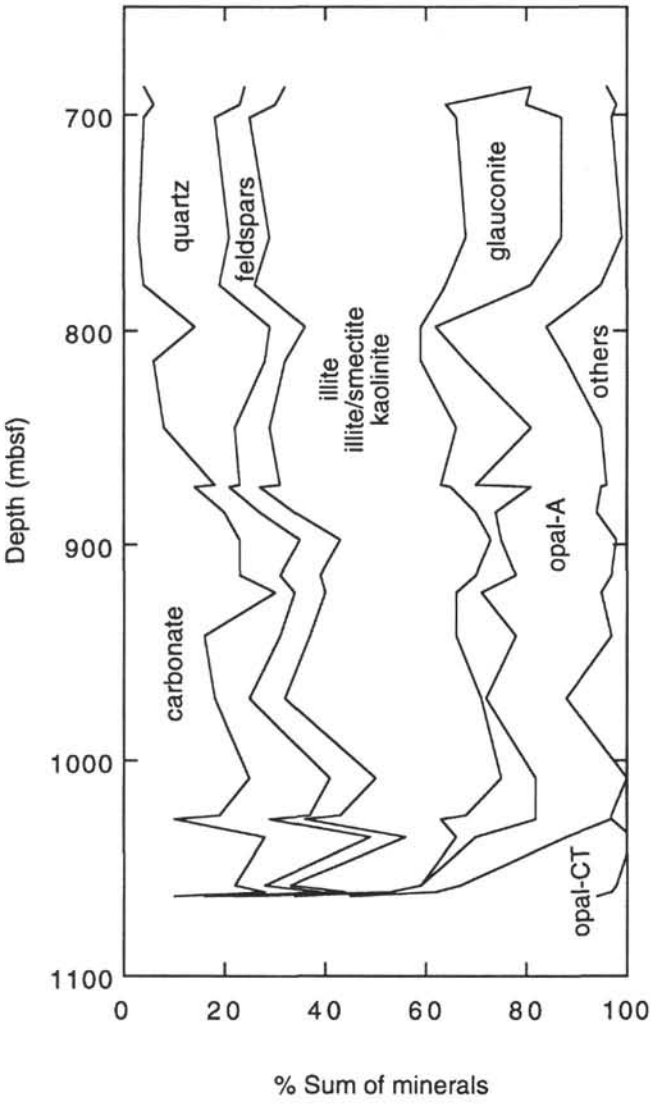

Figure 2. Depth distribution of bulk mineral variations in Hole 903C sediments, determined by XRD.

Precipitation of Opal-CT and the Two Diagenetic "Fronts"

We observed by SEM intermittent occurrences of opal-CT cements in mid-Miocene diatomaceous mudstones (Fig. 6A), through lower Miocene mudstones that contain both partly dissolved diatoms and opal-CT, and down to the upper part of upper Oligocene glauconitic sandy mudstones (Fig. 7A). Despite its relative abundance in SEM observations, quantities detectable by XRD are present only in the lower part of the upper Oligocene (below 1036 mbsf; Fig. 6C, D), where they increase from 0% to ~30% over ~30 m, and even up to 50% over the next 10 m (Fig. 2). This zone of sharp opal-CT increase forms a diagenetic "front" (a term originally keyed for a zone a few meters thick; cf. Thein and von Rad, 1987).

In the samples containing both abundant and relatively well preserved opal-A tests and opal-CT, the opal-CT is probably derived from partial dissolution of opal-A (cf. Williams et al., 1985; Hesse, 1990). Thus, opal-CT precipitation occurred concomitantly with opal-A dissolution. In the upper Eocene chalk, opal-CT is found preferentially at the periphery of large pores but it is less common in the denser matrix of the samples (Fig. 7C, D), suggesting that permeability controlled precipitation. Opal-CT is rare in early diagenetic carbonate concretions, but is present in bands and nodules showing incipient carbonate mineralization. In the latter, opal-CT lepispheres and networks of blades grew on the matrix minerals and on diagenetic carbonates, confirming their late diagenetic origin. Outpourings of diatom dissolution voids by opal-CT lepispheres (Fig. 7B) were less commonly observed. Riech and von Rad (1979) assume that such outpourings formed by an in situ solution-precipitation process.

Our observations support the conclusion that amorphous, biogenic opal-A is always partly or completely dissolved before crystalline opal-CT is precipitated from a solution (Thein and von Rad, 1987; Hesse, 1990). The reaction rate of this process is controlled by time, temperature, and type of host facies (Riech and von Rad, 1979; Isaacs, 1981; Hesse, 1990; Williams et al., 1985): The reaction is generally faster in carbonates and retarded in clay-rich rocks (Kastner et al., 1977). This contrast in bulk mineralogy appears to have controlled the distribution of opal-CT cements at Site 903: Large amounts of opal-CT only occur downward from the basal part of the siliciclastic-dominated upper Oligocene, rich in diagenetic carbonate concretions, and in the upper Eocene chalk. This thick diagenetic front is the most important increase in opal-CT abundance in the sediments drilled at Site 903, and must have modified the character of seismic Reflector o1, generated in part from the siliciclastic/chalk boundary (Shipboard Scientific Party, 1994a; cf. Lorenzo et al., this volume). The front can be traced downslope into the top of the chalk at Site 902 (where no diagenetic carbonate concretions occur right above the top of the chalk), and into a diagenetic horizon (indicated by an opal-CT peak in XRD data; Shipboard Scientific Party, 1994d) at Site 904 (Fig. 8). No opal-CT enrichment was described at the siliciclastic/chalk contact at Sites 612 and 613 (Thein and von Rad, 1987; Wilkens et al., 1987.

In contrast, a diagenetic front within the lower part of the middle Eocene chalks separates semi-indurated chalk (relatively poor in opal-CT) above from porcellanitic chalk (rich in opal-CT) below at Site 904 (Shipboard Scientific Party, 1994d; Fig. 8). An opal-CT peak around 1105 mbsf in Hole 903C (Shipboard Scientific Party, 1994c) indicates the occurrence of a modified lateral equivalent of this front, although opal-CT values decrease again below this depth. Increases in wet-bulk and grain density in the Eocene chalk below 1105 mbsf indicate further compaction and/or cementation at Site 903, although sparry calcite was found to be more common than opal-CT cement below this depth (Shipboard Scientific Party, 1994c). This is corroborated by slightly lower Si/Al ratios below 1100 mbsf (Fig. 3). The formation of the diagenetic front within the Eocene chalk appears to be primarily temperature and time-controlled. The front corresponds to Reflector e2 and is correlated by Lorenzo et al. (this volume) to Reflector A_c on the continental rise off New Jersey where, similarly to Site 904, a diagenetic front separates opal-A bearing (and mostly opal-CT free) sediments above from opal-CT–rich sediments below (Sites 603, 605, 612, and 613; Goldberg et al., 1987; Thein and von Rad, 1987; Wilkens et al., 1987; cf. Tucholke and Mountain, 1979; Fig. 8).

Precipitation of Clinoptilolite

In some samples euhedral clinoptilolite occurs preferentially in large pores such as empty foraminiferal chambers (Fig. 6C). Clinoptilolite was precipitated after opal-CT, which is overgrown by clinoptilolite. Riech and von Rad (1979) found that clinoptilolite preferentially forms during opal-A dissolution or after opal-CT precipitation, and occurs right below the opal-CT diagenetic front within the Eocene chalk in North Atlantic Deep Sea Drilling Project samples. They conclude that clinoptilolite is precipitated from pore waters that contain intermediate dissolved Si concentrations too low for opal-CT or quartz formation. Recent research, however, indicates that clinop-

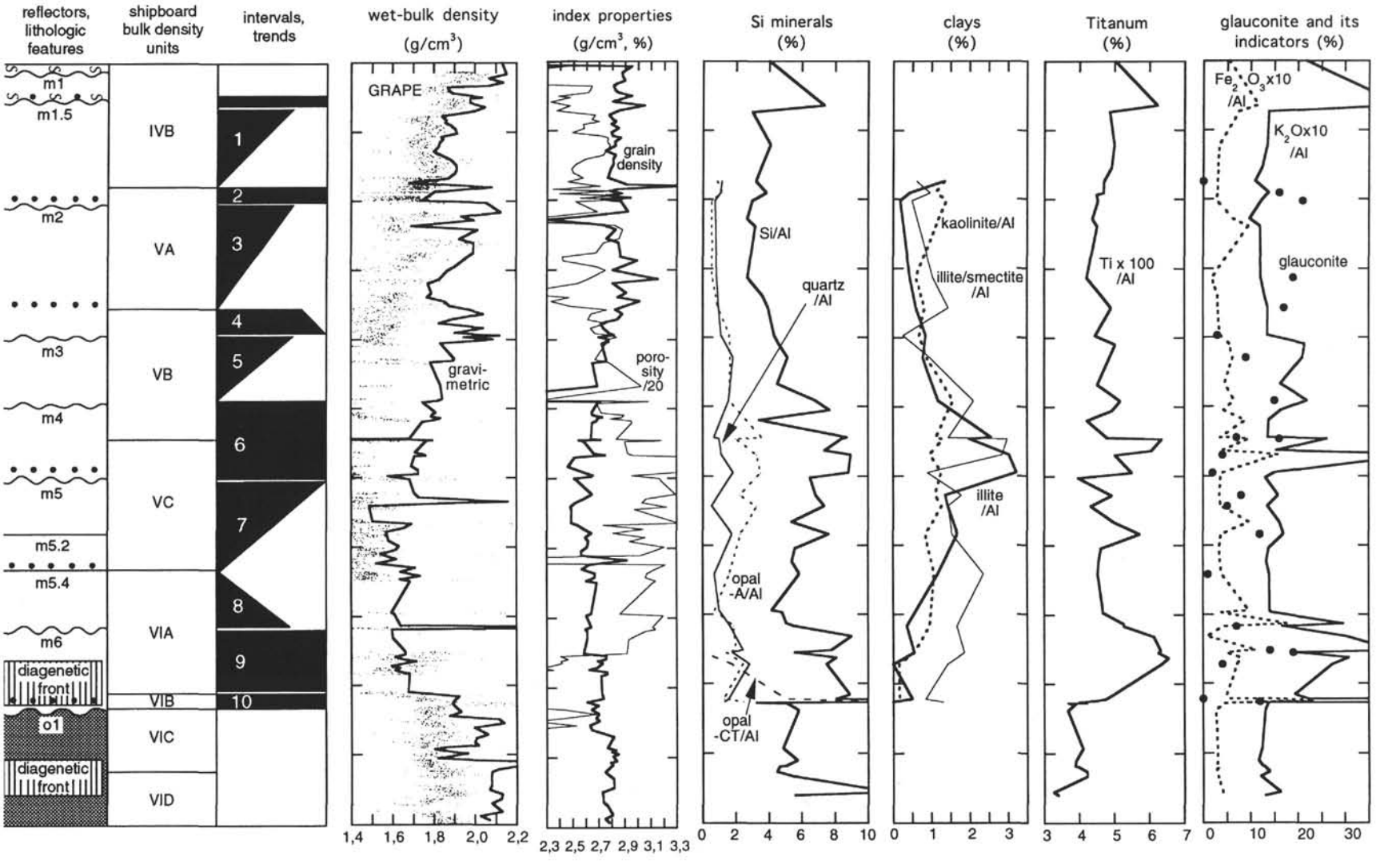

Figure 3. Variations of physical properties, element ratios, and minerals determined by XRD in Miocene–Eocene sediments from Holes 903A (600–700 mbsf) and 903C (700–1150 mbsf). The 10 intervals distinguished on the grounds of covariations in these parameters are shown in black, right margins indicating synthesized patterns (±constant, downhole decreasing, and downhole increasing) in the above-mentioned parameters. Interval 8 is based on Hole 903D data (not shown). Simplified lithology: white = mid-Miocene to upper Oligocene mostly fine-grained siliciclastic sediments, gray = upper–middle Eocene chalk, points = sand units, and S = slumps. Wavy lines = unconformities, straight lines = other reflectors. Opal-CT diagenetic fronts are shown in approximate position. Shipboard bulk density units and physical properties from Shipboard Scientific Party (1994c).

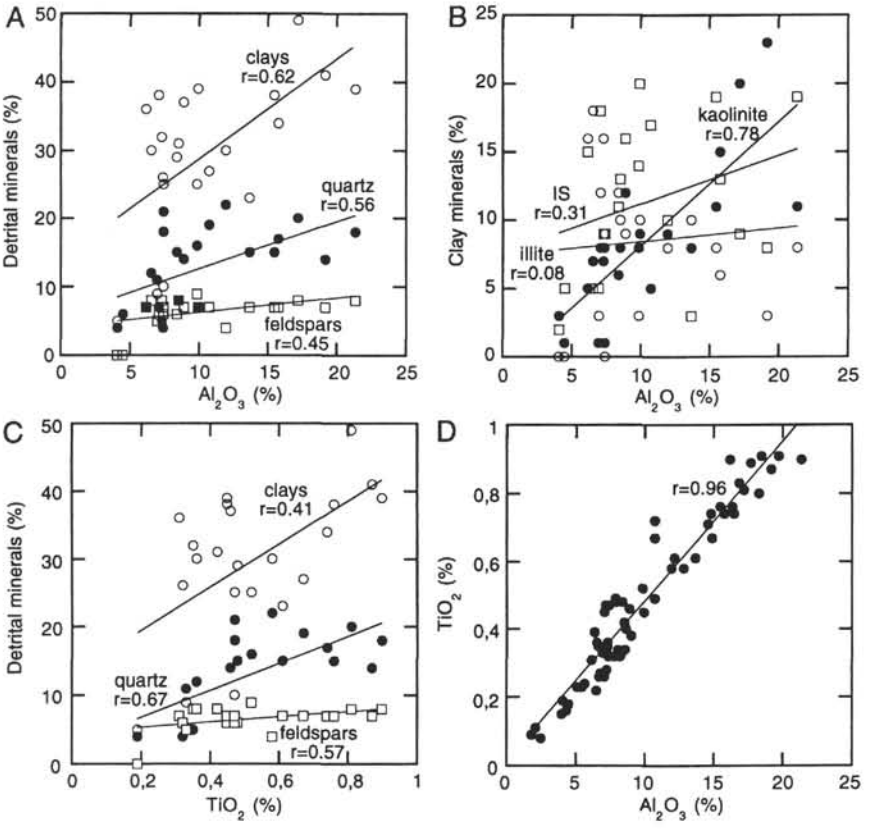

Figure 4. Tests for Al and Ti distribution among the common minerals determined by XRD; r = correlation coefficient. **A.** Al_2O_3 is moderately correlated, in descending order, to the terrigenous minerals (mineral groups) of (total) clays, quartz, and feldspars. **B.** Further resolution of the Al_2O_3 to clays correlation reveals better correlation to kaolinite, lower to illite/smectite, and almost none to illite. **C.** TiO_2 is similarly correlated to the main groups of clay minerals as Al_2O_3. **D.** Excellent correlation of Al_2O_3 to TiO_2.

tilolite precipitation is primarily controlled by the pore water composition (Bohrmann et al., 1989).

PHYSICAL PROPERTIES CYCLES

Cyclic changes are superposed on the general trends of physical properties change in the mid-Miocene to lower Oligocene sediments recovered at Site 903 and are on the order of 100 m or more thick. Cycles are defined by abrupt, steplike offsets in shipboard wet-bulk density records. Five mid-Miocene to lower Oligocene wet-bulk density subunits (labeled IVB, VA, VB, VC, and VIA) were identified by Shipboard Scientific Party (1994c; Fig. 3). Each cycle is characterized by wet-bulk density decreasing more or less continuously downhole by 0.25 g/cm^3. The correspondence of these cycles to sediment properties is confirmed by their covariation with grain density and porosity.

Close observation of the GRAPE wet-bulk density data also reveals cycles approximately 10 m thick superposed on the other trends. The 10-m thickness of these cycles corresponds to the core length, indicating they are drilling artifacts. Each of these small cycles is characterized by higher wet-bulk density in its lower part and lower density in its upper part (variances are approximately 0.1 g/cm^3). No such cycles are evident in the gravimetric measurements although this may be due to larger sampling intervals. The GRAPE density trends indicate compaction in the lower part of the core and/or expansion in its upper part, which probably occurred shortly after the cores were drilled and before they were cut into sections on board. As such, we exclude these small nonsedimentary cycles from our interpretation.

INTERVALS BASED ON PHYSICAL PROPERTIES AND MINERALOGY

Several of the physical properties cycles are composed of two sedimentary and sequence stratigraphic units that could not be separated on the basis of the physical properties data alone because of similar (mostly high) values in two adjacent units. In this section, we overcome this deficiency by considering additional data (mineral contents measured by XRD, and compositional variations indicated by elemental ratios). Thus, we recognize 10 intervals based on different, but frequently covarying, physical properties and/or mineral contents. Additionally, the integration of the visually observed lithologies with mineral composition yields insights into depositional processes. The criteria for correlation of the sequence boundaries from Ew9009 seismic line 1005 (Fig. 9) to the cores and the smear slide data are from Shipboard Scientific Party (1994c). Gravimetric and GRAPE wet-bulk densities covary with grain density unless otherwise stated. Trends are described looking downhole.

Interval 1 (630–690 mbsf): The upper boundary of this interval is overlain by sandy and glauconite-rich sediments, and slumps with high densities and greatly variable porosity; these sediments continue up to and above Unconformity m1. The upper boundary is 5 m below Unconformity m1.5 (which is positioned at the base of a slump/debris flow at 624.5 mbsf) indicating that the sedimentation regime characterized by Interval 1 changed before this mass wasting event. The sediments below the boundary are characterized by lower and further decreasing densities, increasing porosity, and decreasing TiO_2/Al_2O_3 ratio. The basal interval boundary does not correspond to a reflector.

Interval 2 (690–700 mbsf): This thin interval is characterized by high densities and a positive peak in the SiO_2/Al_2O_3 ratio. Although a similar peak in K_2O does not obviously correspond to one in Fe_2O_3, glauconite determined by XRD is high. The base of this density anomaly defines the basal interval boundary and was used, together with a seismic wave velocity high, to locate the position of Unconformity m2.

Interval 3 (700–778 mbsf): Samples from this interval show decreasing wet-bulk density and porosity. For unknown reasons, grain density displays variations with wet-bulk density and porosity opposite to those seen in the other physical properties intervals: Grain densities in Interval 3 increase downhole with decreasing wet-bulk densities and increasing porosities. Low, albeit slightly increasing, $SiO_2/$

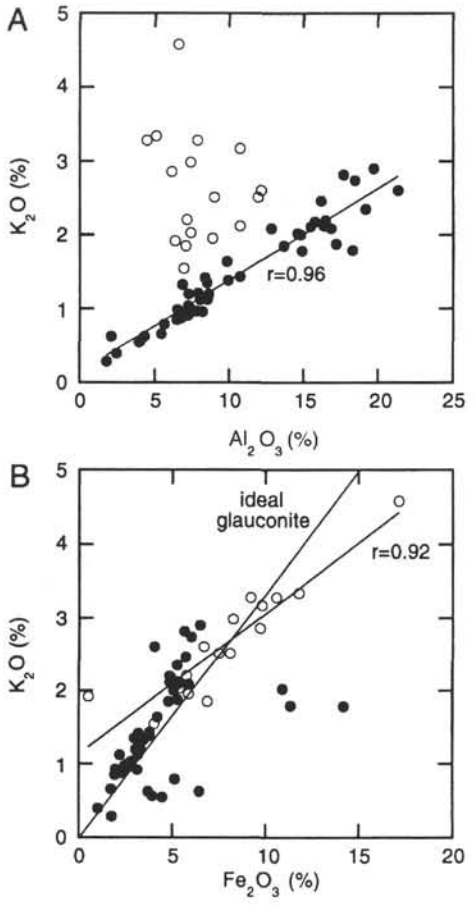

Figure 5. Distinction of glauconite-rich samples by element analysis; r = correlation coefficient. **A.** A group of samples is distinctly, although to varying degrees, enriched in K_2O with respect to Al_2O_3. K_2O and Al_2O_3 are highly correlated in the other samples. **B.** Samples found to be enriched in K_2O with respect to Al_2O_3 show higher and well-correlated Al_2O_3/K_2O ratios, indicating that they are glauconite-rich, although their composition deviates from that of ideal glauconite (composition after Hathaway, 1979). Most samples highly correlated in K_2O/Al_2O_3 are also highly correlated with respect to K_2O/Al_2O_3 ratios.

Al_2O_3 and decreasing TiO_2/Al_2O_3 ratios correlate to low quartz and low but slightly increasing siliceous fossil (opal-A) contents. The main cause of the wet-bulk density and porosity trends is probably increasing opal-A abundance; an increase in siliceous fossils was also found in smear slides. K_2O and Fe_2O_3 contents are generally low, although moderately high glauconite levels were locally determined by XRD. The basal interval boundary is located where trends in wet-bulk density, SiO_2/Al_2O_3 and TiO_2/Al_2O_3 reverse. This boundary corresponds to the base of a thin sand unit and to a reflector of intermediate strength which can be traced updip to just below the shelf where it lies between two thick sediment wedges.

Interval 4 (778–796 mbsf): Wet-bulk densities and SiO_2/Al_2O_3 ratios are high and slightly increase. In addition, smear slide analysis indicates concomitant maxima of quartz and diatom content. The basal interval boundary correlates to the base of a sand unit in Hole 903D, which correlates to Hole 903C at about 796 mbsf. The core density maximum associated with the base of this sand unit defines the position of Unconformity m3.

Interval 5 (796–845 mbsf): Grain and wet-bulk densities decrease, while porosity increases downhole through this interval. This results from a continuation of a broad maximum in siliceous fossils. Elevated, covarying Fe_2O_3 and K_2O values indicate a glauconite maximum. The basal interval boundary is difficult to define using density data alone. Densities continue to decrease through Interval 5 although there are several small, abrupt increases. Based on the density data, the physical properties Subunit VB boundary was positioned farther downcore. Elemental ratios, however, indicate a lower interval boundary at 845 mbsf: SiO_2/Al_2O_3 continues to increase to this depth, apparently owing to increases in both quartz and opal-A contents. This boundary corresponds in depth to sequence boundary m4, which was originally picked at a log velocity maximum.

Interval 6 (845–900 mbsf): Densities continue to decrease through this interval. Porosity increases but does not differ greatly from the overlying sediments. SiO_2/Al_2O_3 ratios are significantly higher than average and continue to increases in the lower samples. This trend is paralleled by a strong increase in opal-A, which again explains the porosity increase. Also in the lower part of the interval, high K_2O and Fe_2O_3 concentrations indicate high glauconite contents. The basal interval boundary corresponds to Unconformity m5, picked at the base of a sand bed and a log velocity increase.

Interval 7 (900–965 mbsf): This interval is characterized by low densities and high porosity. The SiO_2/Al_2O_3 ratio and opal-A content decrease. The interval also has decreasing SiO_2/Al_2O_3 ratios and opal-A concentrations. The covariance of wet-bulk density, grain density, and opal-A decreases is opposite to their relation in the upcore intervals. The large number of pores which remained open after diatom dissolution could explain this relationship. TiO_2/Al_2O_3, K_2O, and Fe_2O_3 show no clear trend, but their peaks distinguish this interval from the underlying one. Interval 7 contains Reflector m5.2, at which no change is observed. The base of the interval is at an offset to slightly higher wet-bulk densities. This boundary, defined at the base of a sand bed, corresponds to Reflector m5.4 at which no unconformable stratal pattern is observed.

Interval 8 (965–1010 mbsf): The trends in this interval are difficult to define in Hole 903C because of substantial missing core. Corresponding cores from Hole 903D show a slight density increase. Low SiO_2/Al_2O_3 ratio and opal-A content are associated with high porosity. The SiO_2/Al_2O_3, K_2O, and Fe_2O_3 data from Hole 903C are low and show little variation. The basal interval boundary is placed at an offset where most trends become significantly higher values. This boundary corresponds to a cemented sand bed that correlates to Unconformity m6.

Interval 9 (1010–1055 mbsf): The SiO_2/Al_2O_3 ratio is offset to a higher level, caused by elevated quartz and opal-A content. However, a rapid increase in opal-CT cements along the diagenetic front whose upper boundary lies within this interval may be another important cause of the jump. The TiO_2/Al_2O_3 ratio also attains high values, indicating a terrigenous mineral composition that significantly differs from most overlying intervals, and is associated with a quartz sand maximum. Glauconite (indicated by high K_2O and Fe_2O_3) is abundant but greatly variable. Grain density increases and porosity sharply decreases within Interval 9. GRAPE wet-bulk density is partly higher than the gravimetric values and may result from concretionary horizons not sampled for gravimetric analyses. Porosity reduction by the opal-A to opal-CT phase transformation probably contributed to the high wet-bulk density. The basal interval boundary is at a step to higher gravimetric density which is, however, absent in the GRAPE trend. This boundary can not be correlated to a reflector on seismic line 1005.

Interval 10 (1055–1064 mbsf): High but decreasing densities and low porosity characterize this interval. The SiO_2/Al_2O_3 and TiO_2/Al_2O_3 ratios and K_2O and Fe_2O_3 values show large variations, which are a function of lithologies with greatly variable glauconite and (commonly coarse-grained) terrigenous minerals content. The basal interval boundary is the top of the Eocene chalk, and corresponds to Reflector o1.

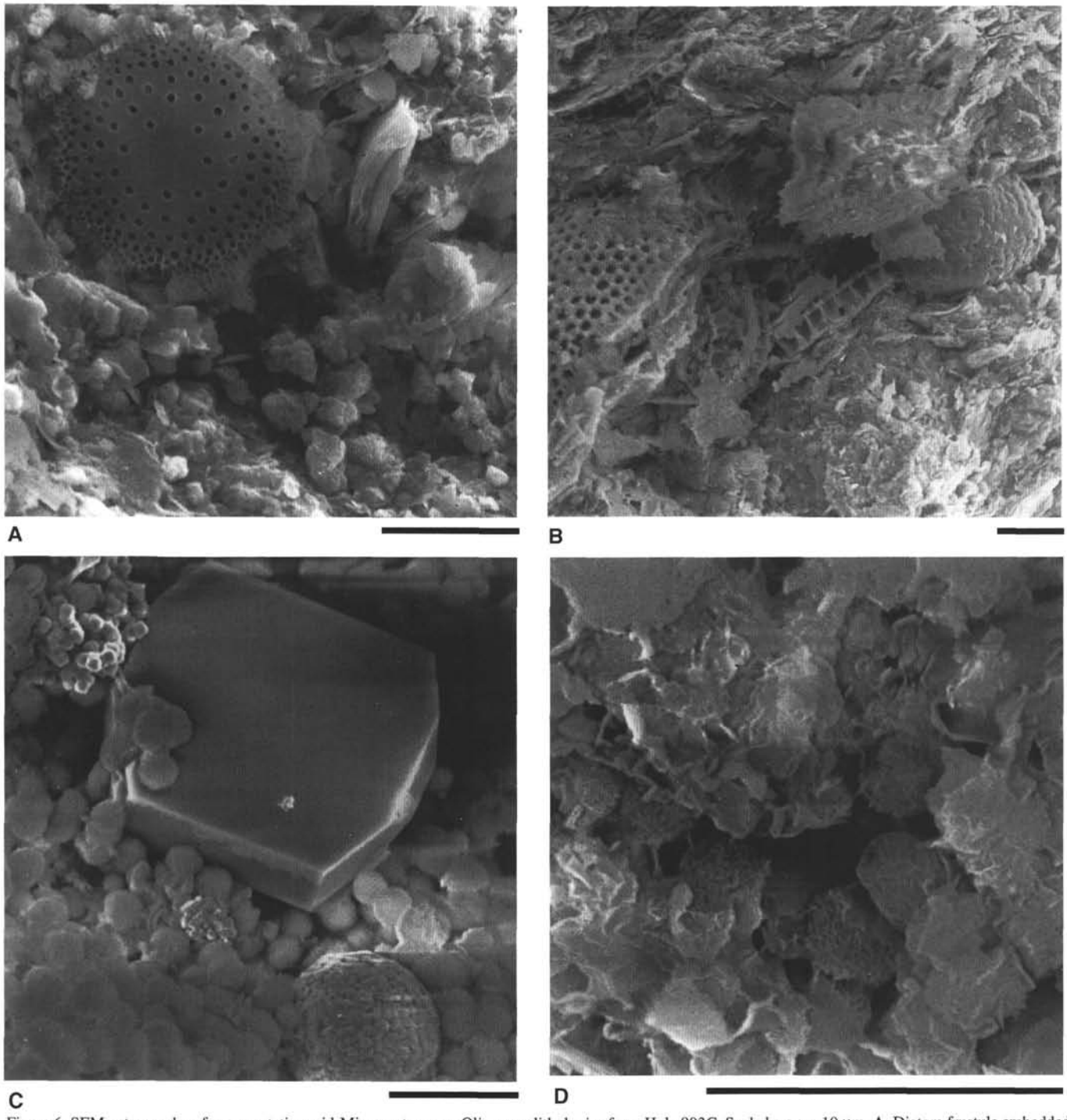

Figure 6. SEM petrography of representative mid-Miocene to upper Oligocene lithologies from Hole 903C. Scale bars are 10 µm. **A.** Diatom frustule embedded in dense matrix composed predominantly of clay minerals. Small opal-CT lepispheres on pore wall in lower right. Sample 150-903C-18R-1, 44–46 cm, middle mid-Miocene. **B.** Sediment rich in fragmented diatom frustules in dense clay-rich matrix. Note the good orientation of platy components ± perpendicular to the vertical and displacive growth of pyrite "framboid." Sample 150-903C-19R-1, 80–82 cm, middle mid-Miocene. **C.** Pore with marginal pyrite framboid is lined by dense layer of opal-CT lepispheres, which are on their turn overgrown by an almost euhedral clinoptilolite crystal. Sample 150-903C-48R-2, 75–77 cm, upper Oligocene. **D.** Strong cementation of clay-rich sediment by interconnecting opal-CT lepispheres and network of blades. Same sample as in Figure 6C.

IMPLICATIONS FOR THE NEW JERSEY MARGIN SEQUENCE STRATIGRAPHY

In this section we relate the trends in the 10 mid-Miocene to upper Oligocene intervals at Site 903 to different seismic facies (Fig. 9), discuss these relationships, and speculate upon their implications to the sequence stratigraphy of the New Jersey continental margin.

Recognition of Systems Tracts at Site 903

Intervals 1, 3, 5, 7, and 8 (all Miocene) are characterized by generally low wet-bulk densities and low non-clay terrigenous mineral contents. There is no clear indication of turbiditic sedimentation; thus, these are probably hemipelagic sediments.

Among these intervals, 1, 3, 5, and 7 show ±linear downcore decreases (i.e., upcore increase) in wet-bulk density and non-clay ter-

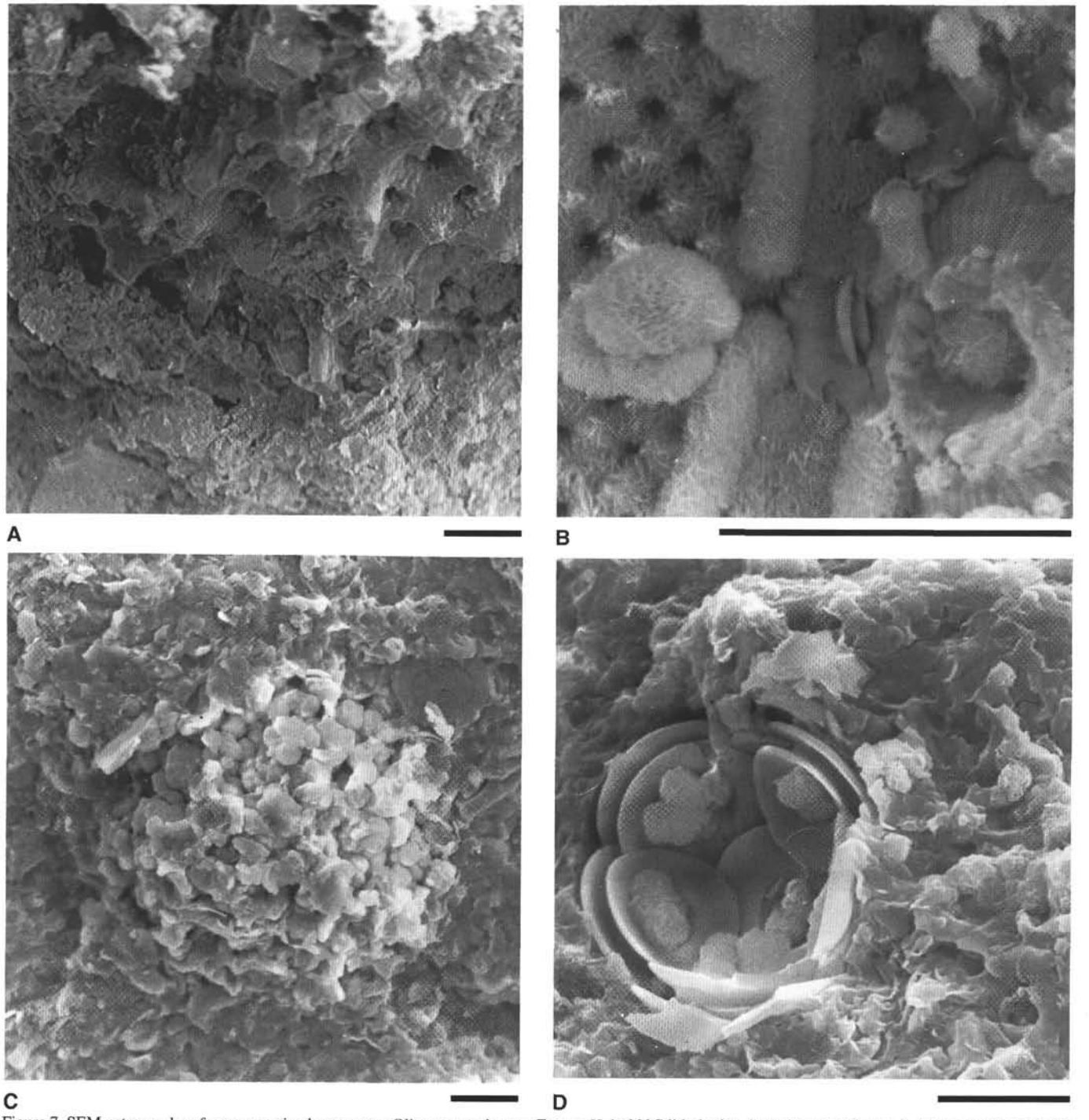

Figure 7. SEM petrography of representative lower upper Oligocene and upper Eocene Hole 903C lithologies. Scale bars are 10 µm. **A.** Large pore in clay-rich sediment generated by complete dissolution of a diatom frustule, whose shape is preserved by the surrounding matrix. Large euhedral mica crystal in lower left. Sample 150-903C-51R-6, 74–77 cm, upper Oligocene, about 3 m above top of the chalk. **B.** Detail of diatom frustule-shaped pore completely filled by opal-CT lepispheres. Small calcite crystals, then opal-CT lepispheres overgrow coccolith and fine-grained matrix on the right. Opal-CT lepispheres overgrow the replaced diatom. Same sample as in Figure 7A. **C.** Matrix of the upper Eocene chalk with coccoliths and fine-grained clay minerals cemented by small calcite crystals. Opal-CT lepispheres preferentially formed in pores, as in dissolved fossil in the center. Sample 150-903C-52R-4, 72–74 cm, about 5 m below top of the chalk. **D.** Detail of chalk matrix with rare coccosphere, partly filled by opal-CT lepispheres. Sample 150-903C-56R-5, 127–130 cm, upper Eocene.

rigenous mineral content. The upcore increase in wet-bulk and grain densities are probably caused by an increase in the terrigenous grains (mainly clays) relative to the volume of diatoms in the sediment. This is probably due to progradation. The upward-increasing trends found in these intervals are also characteristic signatures of natural gamma-ray and spontaneous potential borehole logs of prograding wedges in settings with high sedimentation rates (Mitchum et al., 1993). When placed in a regional depositional perspective (Fig. 9), the intervals correspond to progradational clinoforms indicative of deltaic shelf wedges, or their lateral equivalents (cf. Poag, 1987). The elongate wedges on the seismic section (Intervals 1 and 5) result from the survey cutting the wedges at low angles. Wedges with convex-upward

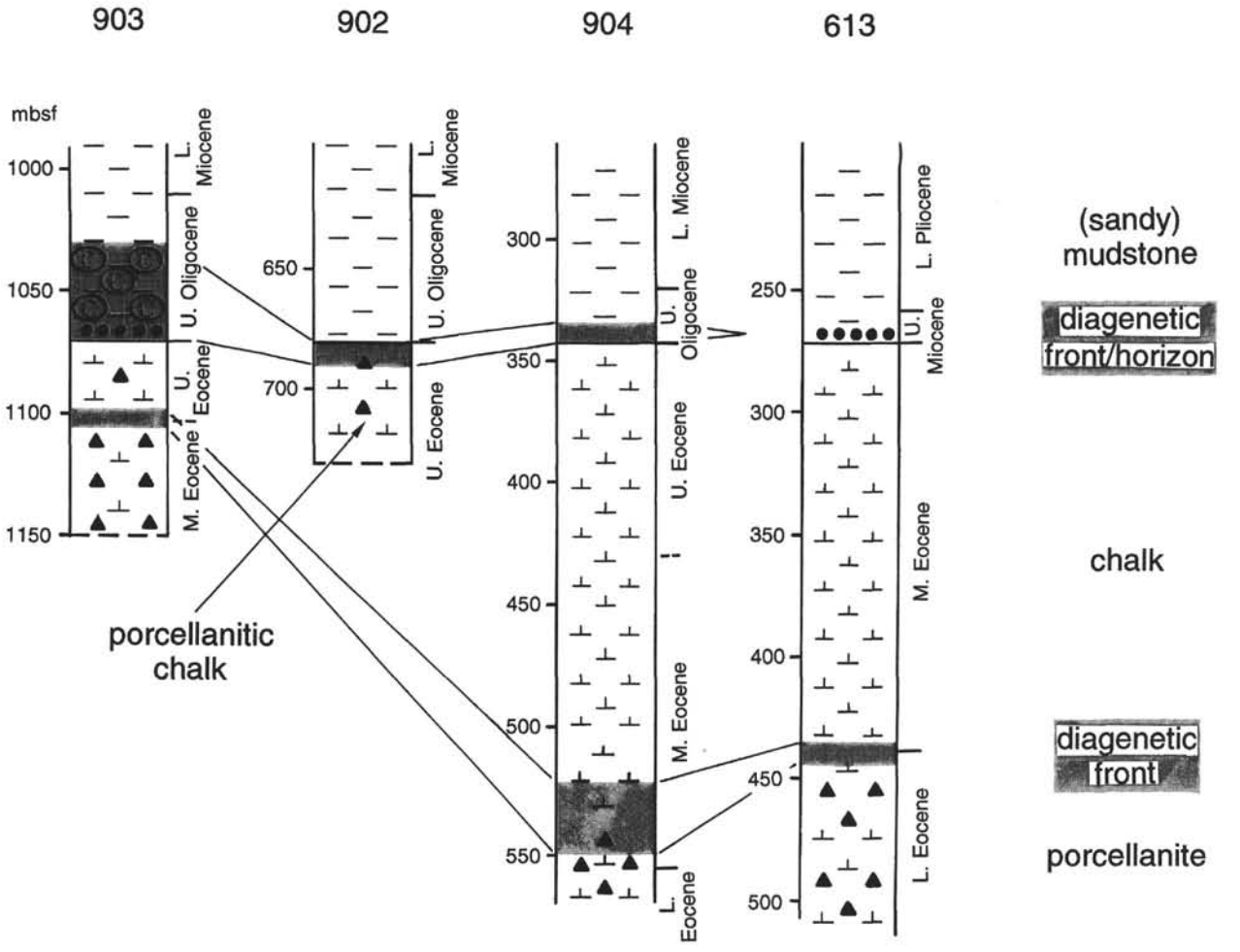

Figure 8. Diagenetic "fronts" resulting from opal-CT precipitation. An upper front occurs above and below the contact upper Oligocene sandy mudstones/upper Eocene chalk at Sites 903 and 902. This front changes downslope into a diagenetic horizon at Site 904 and was not found at Site 613. A lower front occurs between downslope progressively older parts of the chalk at all Sites. Black dots = sand-rich interval, and encircled C = zone of early diagenetic carbonate concretions. Based on lithologic descriptions and XRD analyses from Shipboard Scientific Party (1994b, 1994c, 1994d), Thein and von Rad (1987), and our XRD results.

("mounded") geometry (Intervals 3 and 7) fill the relief created seaward of the older wedges and result from the survey cutting them at high angles to the main progradation direction.

Interval 8 differs by slightly downcore increasing (i.e., upcore decreasing) density, which may indicate progradation away from Site 903. However, our physical properties and compositional indicators are less well defined in this interval, and thus this interpretation is tentative.

Intervals 2, 4, 6 (Miocene) and 9 and 10 (upper Oligocene) are characterized by high wet-bulk density and/or abundant non-clay terrigenous minerals and, to a lesser extent, by a high glauconite content. Coarse grain sizes (sands) are also common.

Two intervals from this group can be traced below the shelf (Interval 4) or farther downslope (Interval 2) into prograding wedges, indicating deposition seaward or laterally from these wedges (Fig. 9). Interval 2 occurs at the base of a prograding wedge, and corresponds in stratigraphic position and inferred lithology to a lowstand fan. Because Interval 2 is very thin, it is not resolved on the available seismic lines. High and constant borehole gamma-ray log trends, similar to those seen in these intervals, are typical for deep-sea fans deposited during sea-level lowstands (Mitchum et al., 1993). The lithology of cores recovered through these intervals are also in accordance with the postulates for passive-margin deep-sea fans. Lithologies in these fans are thought to consist of relatively coarse and commonly winnowed sediments, transported to the deep sea by sediment gravity flow (Vail et al., 1977; Van Wagoner et al., 1988).

Interval 4 differs from others in this group by high and slightly upcore decreasing densities. The causes of the trend in this interval are incompletely understood. However, laterally correlative progradation, visible on the regional seismic lines below the shelf, indicates that the cause of the upcore decreasing wet-bulk density trend may be progradation away from Site 903.

Interval 6 (Miocene) and the upper Oligocene Intervals 9 and 10 are thin units between laterally continuous reflectors. The reflectors retain this character over several tens of kilometers below the shelf perpendicular and, at least in the Oligocene, also parallel to the New Jersey Margin (cf. Poag, 1987; Fulthorpe et al., this volume). Considering these properties and the lithology, Interval 6 probably represents a winnowed lowstand fan. Intervals 9 and 10 represent distal slope sediments, which we cannot attribute to systems tracts.

Sequences of the Prograding Continental Margin

Greenlee et al. (1992), using seismic, logging, and core data, showed that the Neogene depositional sequences on the New Jersey continental margin consist of relatively thin lowstand fans, present

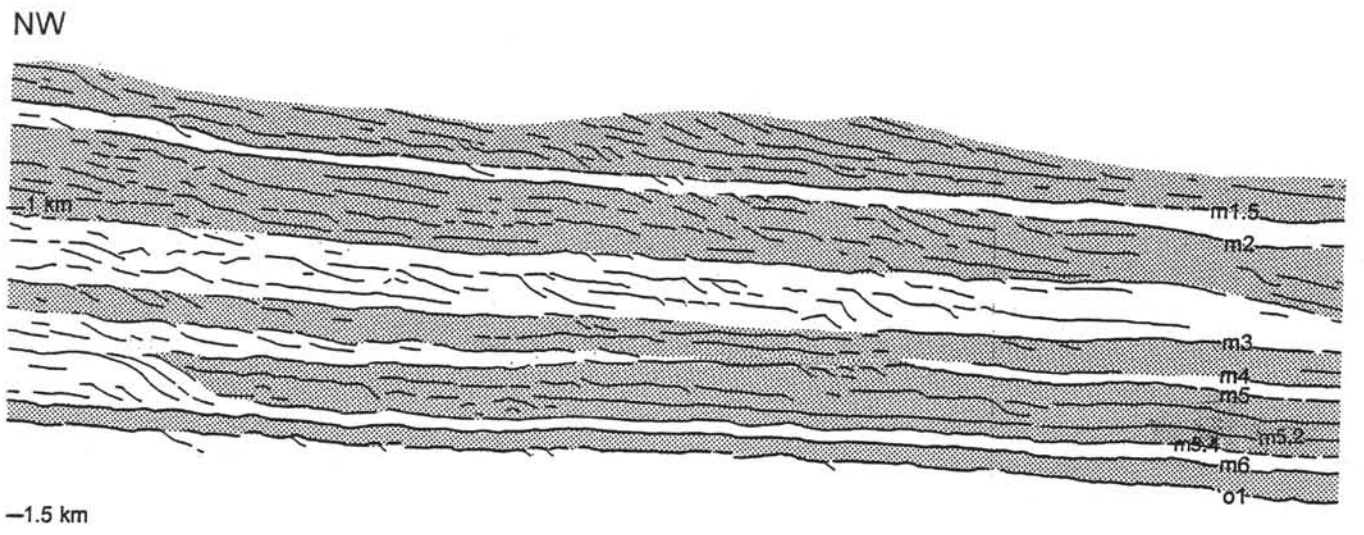

Figure 9. Interpretation of depth-converted seismic section (Ew9009 Line 1005, segment 72.96°W/39.02°N to 72.73°W/38.89°N; cf. Fig. 1) normal to the New Jersey continental margin and intervals defined by physical properties and mineralogical variations (numbered 1 to 10). Reflectors m1, m1.5, m2, m3, m4, m5, m6, and o1 are unconformable depositional sequence boundaries that can be traced below the shelf; Reflectors m5.2 and m5.4 and an uncoded reflector between Units 3 and 4 are conformable boundaries between systems tracts (e.g., transgressive surfaces). Thick highstand and lowstand prograding wedges cut at different angles (Intervals 1, 3, 5, 6, and 7) increasingly replace upsection units between thin and laterally continuous reflectors or units too thin to have caused a reflector (Intervals 2, and 9 and 10, interpreted as lowstand fans and as distal slope sediments). Interval 4 occurs at a facies transition. Interval 8 combines parallel seismic facies and upward decreasing values. Straight and inclined interval edges symbolize trends in parameters (cf. Fig. 3). Geometries of sequence boundaries from Shipboard Scientific Party (1994a).

along their sections in some of the sequences only, and of two thick prograding lowstand and highstand wedges (Fig. 10). Along the strike of the continental margin, these fans pinch out laterally and partly overlie each other (Poag, 1987; McMaster et al., 1989). Because the rate of sediment input greatly exceeded the rate of accommodation, sediments of the transgressive systems tract are thin or absent in these sequences (Greenlee et al., 1992). Considering the distal position of Site 903 with respect to the depocenters of the Oligocene and the subsequent progradation of the lower and mid-Miocene depocenters toward Site 903 (cf. Poag, 1987), it is not surprising that the thickness and completeness of the sequences generally increases upsection along with sedimentation rates (~60 cm/k.y. in the middle–late Miocene; Shipboard Scientific Party, 1994c).

We now integrate the reflector (i.e., stratal) geometries and the position of sequence boundaries from the seismic section (Ew9009 line 1005; Fig. 9; Shipboard Scientific Party, 1994a) with the depositional style of the intervals (Fig. 10). Thus, the Miocene Intervals 1 to 8 can be grouped into five depositional sequences. The differences in the systems tracts reflect lateral variations in the sequences (cf. Poag and Mountain, 1987). Unconformable stratal patterns (e.g., truncation), as well as more and longer depositional hiatuses, occur along the sequence boundaries, although patterns are conformable along the other systems tracts boundaries (e.g., transgressive surfaces; Miller et al., this volume; Table 3).

Intervals 1 and 2 correspond to one depositional sequence. This sequence consists of a basal lowstand fan (Interval 2), which is overlain by a lowstand or highstand prograding wedge (Interval 1).

Intervals 3 and 4, and 7 and 8, were defined as depositional sequences composed of one basal lowstand prograding wedge overlain by a highstand wedge which prograded further. The highstand wedge laterally from Interval 3 is divided in two (the separation is around the label "m2" on Fig. 9), with geometries indicating changing progradation directions, possibly due to delta switching. Interpretation of Intervals 4 and 8 as the distal parts of prograding wedges indicates that the downward increasing (i.e., upward decreasing) trends may have been caused by progradation away from Site 903. The observed trends contrast with the upward increase commonly caused by progradation. According to our interpretation, m5.2 is the only important reflector along our seismic section which does not correspond to a sequence or systems tract boundary.

We interpret Interval 6, and the upper Oligocene intervals (9 and 10) together, as lowstand fans and as distal slope sediments that each correspond to one seismic and lithostratigraphically defined sequence. However, a sequence boundary between Intervals 9/10 may remain unrecognized because of a conformable reflector pattern.

The five Miocene sequences along our seismic section correspond to the same number of sequences proposed by Greenlee et al. (1992) for this time along a transect parallel to our section. However, they place the top of the uppermost of these sequences at Unconformity m1 (= tuscan), within the unit of sands and slumps overlying the Intervals 1/2 boundary (Fig. 3). In the upper Oligocene, meaningful comparison is as yet difficult because of incomplete age constraints (cf. Miller et al., 1990).

CONCLUSIONS

We integrated the systematic variations in physical properties (GRAPE and gravimetric wet-bulk densities, grain density, and porosity) and mineralogical characteristics (determined by XRD and inferred from element analyses) to subdivide the mid-Miocene to upper Oligocene at Site 903 into 10 intervals. Each interval is characterized by a distinct combination of physical and mineralogical properties that are interpreted to reflect primarily changes in the proportions of various terrigenous minerals, biogenic frustules and shells (mostly diatoms), and pores. This approach demonstrates how the interpretation of systematic (often cyclic) physical properties variations can contribute to understanding sedimentation and sequence stratigraphy

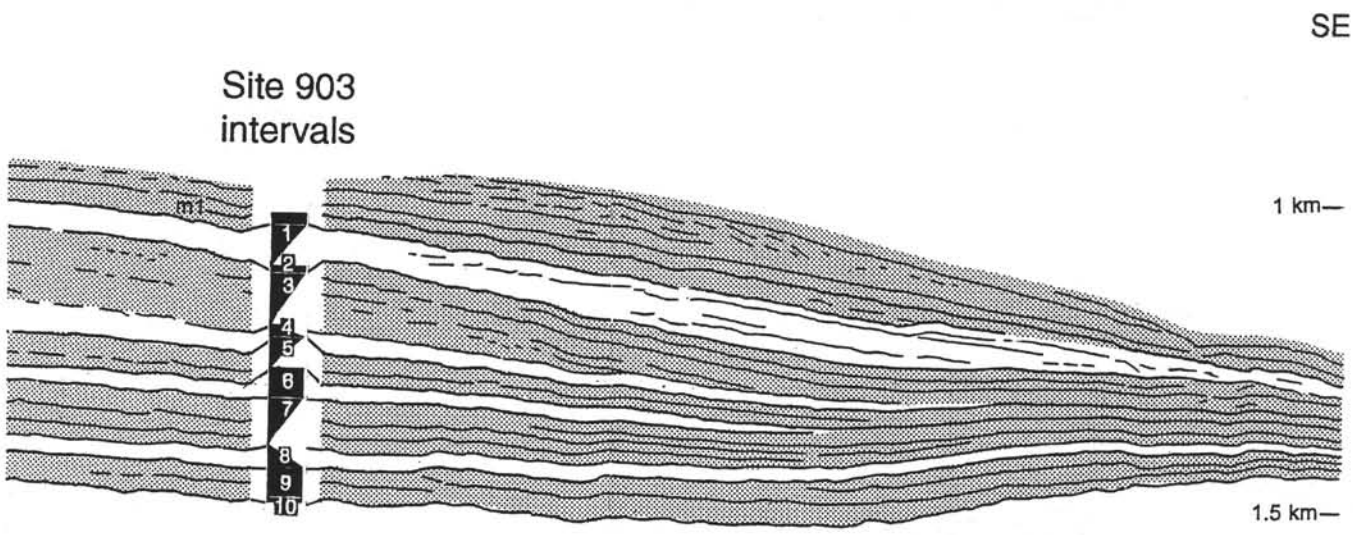

Figure 9 (continued).

in fine-grained sediments. It also shows, however, that using one highly resolved parameter alone (e.g., gravimetric and GRAPE wet-bulk densities) can result in still insufficient resolution. Another data set (mineral composition) was needed to attain a resolution that allowed better integration with the results of seismic interpretation. Onboard core logging of natural gamma-ray emissions, introduced during Leg 150 but incomplete for Site 903 (Hoppie, Blum, et al., 1994), promises to yield such a data set, which can be interpreted with respect to clay mineral content.

Further integration of the 10 intervals with the seismic facies, sequence boundaries, and visual lithostratigraphy suggests that the eight lower to mid-Miocene intervals correspond to the lowstand and highstand systems tracts of five depositional sequences along a seismic section normal to the New Jersey Margin. We interpret the intervals characterized by high density and high terrigenous non-clay minerals contents as (winnowed) lowstand fans. The intervals characterized by low and upward increasing density and (often co-) varying mineralogy, abundant in clays and siliceous fossils, correspond to prograding deltaic wedges. Two upper Oligocene intervals are thought to represent winnowed distal slope sediments.

These analyses contribute to understanding the internal organization and sedimentological character of most sequences recognized below the New Jersey shelf and slope by Greenlee et al. (1992), thus corroborating the validity of their model. However, interpretation of the high-resolution seismics alone was insufficient to obtain such results. The generally increasing thickness and increasing internal resolution of the sequences from the upper Oligocene to the mid-Miocene reflects higher sedimentation rates and changing sediment types as the continental margin prograded.

ACKNOWLEDGMENTS

G. Mountain, R.H. Wilkens, and H. Yin reviewed the manuscript and made valuable suggestions for its improvement. G. Mountain provided the seismic section. G. Bohrmann kindly commented on clinoptilolite formation. J. Otto provided XRF analytical facilities. S. Dachnowsky, J. Loritz, and H. Schlegel aided with the element analyses. K.-H. Gräf carried out the photographic work. R. Schlenker helped in sample preparation and drafting. We also thankfully acknowledge funding by the Deutsche Forschungsgemeinschaft to A.V. (grant Ve 146/3-1), and by the U.S. Science Support Program to B.W.H. (Account No. 150-20783a).

REFERENCES

Bennett, R.H., O'Brien, N.R., and Hulbert, M.H., 1991. Determinants of clay and shale microfabric signatures: processes and mechanisms. *In* Bennett, R.H., Bryant, W.R., and Hulbert, M.H. (Eds.), *Microstructure of Fine-Grained Sediments: From Mud to Shale:* New York (Springer-Verlag), 5–32.

Bohrmann, G., Stein, R., and Faugères, J.-C., 1989. Authigenic zeolites and their relation to silica diagenesis in ODP Site 661 sediments (Leg 108, eastern equatorial Atlantic). *Geol. Rundsch.,* 78:779–792.

Boyce, R.E., 1973. Physical properties—methods. *In* Edgar, N.T., Saunders, J.B., et al., *Init. Repts. DSDP,* 15: Washington (U.S. Govt. Printing Office), 1115–1128.

———, 1976. Definitions and laboratory techniques of compressional sound velocity parameters and wet-water content, wet-bulk density, and porosity parameters by gravimetric and gamma-ray attenuation techniques. *In* Schlanger, S.O., Jackson, E.D., et al., *Init. Repts. DSDP,* 33: Washington (U.S. Govt. Printing Office), 931–958.

Busch, W.H., 1991. Analysis of wet-bulk density and sediment color cycles in Pliocene–Pleistocene sediments of the Owen Ridge (Site 722) and Oman Margin (Site 728). *In* Prell, W.L., Niitsuma, N., et al., *Proc. ODP, Sci. Results,* 117: College Station, TX (Ocean Drilling Program), 239–253.

Christie-Blick, N., Mountain, G.S., and Miller, K.G., 1990. Seismic stratigraphic record of sea-level change. *In* National Research Council, *Studies in Sea-Level Change:* Washington (National Academy Press), 116–140.

Frakes, L.A., Francis, J.E., and Syktus, J.I., 1992. *Climate Modes of the Phanerozoic:* Cambridge (Cambridge Univ. Press).

Goldberg, D., Wilkens, R.H., and Moos, D., 1987. Seismic modeling of diagenetic effects in Cenozoic marine sediments at Deep Sea Drilling Project Sites 612 and 613. *In* Poag, C.W., Watts, A.B., et al., *Init. Repts. DSDP,* 95: Washington (U.S. Govt. Printing Office), 589–599.

Greenlee, S.M., Devlin, W.J., Miller, K.G., Mountain, G.S., and Flemings, P.B., 1992. Integrated sequence stratigraphy of Neogene deposits, New Jersey continental shelf and slope: comparison with the Exxon model. *Geol. Soc. Am. Bull.,* 104:1403–1411.

Greenlee, S.M., and Moore, T.C., 1988. Recognition and interpretation of depositional sequences and calculation of sea level changes from stratigraphic data—offshore New Jersey and Alabama Tertiary. *In* Wilgus, C.K., Posamentier, H., Ross, C.A., and Kendall, C.G.St.C. (Eds.), *Sea Level Changes: An Integrated Approach.* Spec. Publ.—Soc. Econ. Paleontol. Mineral., 42:329–353.

Greenlee, S.M., Schroeder, F.W., and Vail, P.R., 1988. Seismic stratigraphic and geohistory analysis of Tertiary strata from the continental shelf off New Jersey: calculation of eustatic fluctuations from stratigraphic data. *In* Sheridan, R.E., and Grow, J.A. (Eds.), *The Atlantic Continental Margin.* Geol. Soc. Am., Geol. of North Am. Ser., 437–444.

Hack, J.T., 1982. Physiographic divisions and differential uplift in the Piedmont and Blue Ridge. *Geol. Surv. Prof. Pap. (U.S.),* 1265.

Hamilton, E.L., 1976. Variations of density and porosity with depth in deep-sea sediments. *J. Sediment. Petrol.,* 46:280–300.

Hathaway, J.C., 1979. Clay minerals. *In* Burns, R.G. (Ed.), *Marine Minerals.* Short Course Notes—Mineral. Soc. Am., 6:123–148.

Hesse, R., 1990. Origin of chert: diagenesis of biogenic siliceous sediments. *In* McIlreath, I.A., and Morrow, D.W. (Eds.), *Diagenesis.* Geosci. Can. Reprint Ser., 4:227–251.

Hoppie, B.W., Blum, P., and the Shipboard Scientific Party, 1994. Natural gamma-ray measurements on ODP cores: introduction to procedures with examples from Leg 150. *In* Mountain, G.S., Miller, K.G., Blum, P., et al., *Proc. ODP, Init. Repts.,* 150: College Station, TX (Ocean Drilling Program), 51–59.

Hurd, D.C., and Theyer, F., 1977. Changes in the physical and chemical properties of biogenic silica from the central equatorial Pacific, Part II. Refraction index, density, and water content of acid cleaned samples. *Am. J. Sci.,* 227:1168–1202.

Isaacs, C.M., 1981. Porosity reduction during diagenesis of the Monterey Formation, Santa Barbara coastal area, California. *In* Garrison, R.E., Douglas, R.G., Pisciotto, K.E., Isaacs, C.M., and Ingle, J.C. (Eds.), *The Monterrey Formation and Related Siliceous Rocks of California.* Spec. Publ.—Soc. Econ. Paleontol. Mineral., Pacific Sect., 257–271.

Kastner, M., Keene, J.B., and Gieskes, J.M., 1977. Diagenesis of siliceous oozes, I. Chemical controls on the rate of opal-A to opal-CT transformation—an experimental study. *Geochim. Cosmochim. Acta,* 41:1041–1059.

Mayer, L.A., 1991. Extraction of high-resolution carbonate data for paleoclimate reconstruction. *Nature,* 352:148–150.

Mayer, L.A., Jansen, E., Backman, J., and Takayama, T., 1993. Climatic cyclicity at Site 806: the GRAPE record. *In* Berger, W.H., Kroenke, L.W., Mayer, L.A., et al., *Proc. ODP, Sci. Results,* 130: College Station, TX (Ocean Drilling Program), 623–639.

McMaster, R.L., Locker, S.D., and Laine, E.P., 1989. The early Neogene continental rise off the eastern United States. *Mar. Geol.,* 87:137–163.

Miller, K.G., et al., 1994. *Proc. ODP, Init. Repts.,* 150X: College Station, TX (Ocean Drilling Program).

Miller, K.G., Kent, D.V., Brower, A.N., Bybell, L.M., Feigenson, M.D., Olsson, R.K., and Poore, R.Z., 1990. Eocene–Oligocene sea-level changes on the New Jersey coastal plain linked to the deep-sea record. *Geol. Soc. Am. Bull.,* 102:331–339.

Miller, K.G., and Mountain, G.S., 1994. Global sea-level change and the New Jersey margin. *In* Mountain, G.S., Miller, K.G., Blum, P., et al., *Proc. ODP, Init. Repts.,* 150: College Station, TX (Ocean Drilling Program), 11–20.

Miller, K.G., Wright, J.D., and Fairbanks, R.G., 1991. Unlocking the Ice House: Oligocene–Miocene oxygen isotopes, eustasy, and margin erosion. *J. Geophys. Res.,* 96:6829–6848.

Mitchum, R.M., Sangree, J.B., Vail, P.R., and Wornardt, W.W., 1993. Recognizing sequences and systems tracts from well logs, seismic data, and biostratigraphy: examples from the late Cenozoic of the Gulf of Mexico. *In* Weimer, P., and Posamentier, H. (Eds.), *Siliciclastic Sequence Stratigraphy: Recent Developments and Applications.* AAPG Mem., 58:163–197.

Moon, C.F., and Hurst, C.W., 1984. Fabrics of muds and shales: an overview. *In* Stow, D.A.V., and Piper, D.J.W. (Eds.), *Fine-Grained Sediments: Deep-Water Processes and Facies.* Geol. Soc. Spec. Publ. London, 15:579–593.

Mountain, G.S., and Tucholke, B.E., 1985. Mesozoic and Cenozoic geology of the U.S. Atlantic continental slope and rise. *In* Poag, C.W. (Ed.), *Geologic Evolution of the United States Atlantic Margin:* New York (Van Nostrand Reinhold), 293–341.

Murray, R.W., Leinen, M., and Isern, A.R., 1993. Biogenic flux of Al to sediment in the central equatorial Pacific Ocean: evidence for increased productivity during glacial periods. *Paleoceanography,* 8:651–670.

Nobes, D.C., Murray, R.W., Kuramoto, S., Pisciotto, K.A., and Holler, P., 1992. Impact of silica diagenesis on physical property variations. *In* Pisciotto, K.A., Ingle, J.C., Jr., von Breymann, M.T., Barron, J., et al., *Proc. ODP, Sci. Results,* 127/128 (Pt. 1): College Station, TX (Ocean Drilling Program), 3–31.

O'Brien, N.R., 1987. The effects of bioturbation on the fabric of shale. *J. Sediment. Petrol.,* 57:449–455.

Olhoeft, G.R., and Johnson, G.R, 1989. Densities of rocks and minerals. *In* Carmichael, R.S. (Ed.), *Practical Handbook of Physical Properties of Rocks and Minerals:* Boca Raton (CRC Press), 139–176.

Poag, C.W., 1985. Cenozoic and Upper Cretaceous sedimentary facies and depositional systems of the New Jersey slope and rise. *In* Poag, C.W. (Ed.), *Geological Evolution of the United States Atlantic Margin:* New York (Van Nostrand Reinhold), 343–365.

————, 1987. The New Jersey transect: stratigraphic framework and depositional history of a sediment-rich passive margin. *In* Poag, C.W., Watts, A.B., et al., *Init. Repts. DSDP,* 95: Washington (U.S. Govt. Printing Office), 763–817.

Poag, C.W., and Mountain, G.S., 1987. Late Cretaceous and Cenozoic evolution of the New Jersey continental slope and upper rise: an integration of borehole data with seismic reflection profiles. *In* Poag, C.W., Watts, A.B., et al., *Init. Repts. DSDP,* 95: Washington (U.S. Govt. Printing Office), 673–724.

Ramsay, A.T.S., 1973. A history of organic siliceous sediments in the oceans. *In* Hughes, N.F. (Ed.), *Spec. Pap. Paleontol.,* 12:199–234.

Riech, V., and von Rad, U., 1979. Silica diagenesis in the Atlantic Ocean: diagenetic potential and transformations. *In* Talwani, M., Hay, W., and Ryan, W.B.F. (Eds.), *Deep Drilling Results in the Atlantic Ocean: Continental Margins and Paleoenvironment.* Am. Geophys. Union, Maurice Ewing Ser., 3:315–340.

Robert, P., 1985. *Histoire Géthermique et Diagenèse Organique:* Pau (Elf-Aquitaine).

Rösler, H.J., 1981. *Lehrbuch der Mineralogie:* Leipzig (Verlag für Grundstoffindustrie).

Schlee, J.S., 1981. Seismic stratigraphy of Baltimore Canyon Trough. *AAPG Bull.,* 65:26–53.

Schlee, J.S., and Hinz, K., 1987. Seismic stratigraphy and facies of continental slope and rise seaward of Baltimore Canyon Trough. *AAPG Bull.,* 71:1046–1067.

Shipboard Scientific Party, 1994a. Explanatory notes. *In* Mountain, G.S., Miller, K.G., Blum, P., et al., *Proc. ODP, Init. Repts.,* 150: College Station, TX (Ocean Drilling Program), 21–42.

————, 1994b. Site 902. *In* Mountain, G.S., Miller, K.G., Blum, P., et al., *Proc. ODP, Init. Repts.,* 150: College Station, TX (Ocean Drilling Program), 63–127.

————, 1994c. Site 903. *In* Mountain, G.S., Miller, K.G., Blum, P., et al., *Proc. ODP, Init. Repts.,* 150: College Station, TX (Ocean Drilling Program), 129–205.

————, 1994d. Site 904. *In* Mountain, G.S., Miller, K.G., Blum, P., et al., *Proc. ODP, Init. Repts.,* 150: College Station, TX (Ocean Drilling Program), 207–253.

Steckler, M.S., Reynolds, D.J., Coakley, B.J., Swift, B.A., and Jarrard, R., 1993. Modelling passive margin sequence stratigraphy. *In* Posamentier, H.W., Summerhayes, C.P., Haq, B.U., and Allen, G.P. (Eds.), *Sequence Stratigraphy and Facies Associations.* Spec. Publ. Int. Assoc. Sedimentol., 18:19–41.

Thein, J., and von Rad, U., 1987. Silica diagenesis in continental rise and slope sediments off eastern North America (Sites 603 and 605, Leg 93; Sites 612 and 614, Leg 95). *In* Poag, C.W., Watts, A.B., et al., *Init. Repts. DSDP,* 95: Washington (U.S. Govt. Printing Office), 501–525.

Thiede, J., 1981. Sedimentation und physiographische Entwicklung des Nordatlantiks seit dem mittleren Mesozoikum. *Geol. Rundsch.,* 70:316–326.

Tucholke, B.E., and Mountain, G.S., 1979. Seismic stratigraphy, lithostratigraphy, and paleosedimentation patterns in the North American basin. *In* Talwani, M., Hay, W., and Ryan, W.B.F. (Eds.), *Deep Drilling Results in the Atlantic Ocean: Continental Margins and Paleoenvironment.* Am. Geophys. Union, Maurice Ewing Ser., 3:58–86.

Vail, P.R., Mitchum, R.M., Jr., Todd, R.G., Widmier, J.M., Thompson, S., III, Sangree, J.B., Bubb, J.N., and Hatlelid, W.G., 1977. Seismic stratigraphy and global changes in sea level. *In* Payton, C.E. (Ed.), *Seismic Stratigraphy—Applications to Hydrocarbon Exploration.* AAPG Mem., 26:49–143.

Van Wagoner, J.C., Posamentier, H.W., Mitchum, R.M., Jr., Vail, P.R., Sarg, J.F., Loutit, T.S., and Hardenbol, J., 1988. An overview of the fundamentals of sequence stratigraphy and key definitions. *In* Wilgus, C.K., Hastings, B.S., Ross, C.A., Posamentier, H.W., Van Wagoner, J., and

Kendall, C.G.St.C. (Eds.), *Sea-Level Changes: An Integrated Approach.* Spec. Publ.—Soc. Econ. Paleontol. Mineral., 42:39–45.

Wilkens, R.H., Schreiber, B.C., Caruso, L., and Simmons, G., 1987. The effects of diagenesis on the microstructure of Eocene sediments bordering the Baltimore Canyon Trough. *In* Poag, C.W., Watts, A.B., et al., *Init. Repts. DSDP,* 95: Washington (U.S. Govt. Printing Office), 527–547.

Williams, L.A., Parks, G. A., and Crerar, D. A., 1985. Silica diagenesis, I. Solubility controls. *J. Sediment. Petrol.,* 55:301–311.

Date of initial receipt: 6 March 1995
Date of acceptance: 17 October 1995
Ms 150SR-026

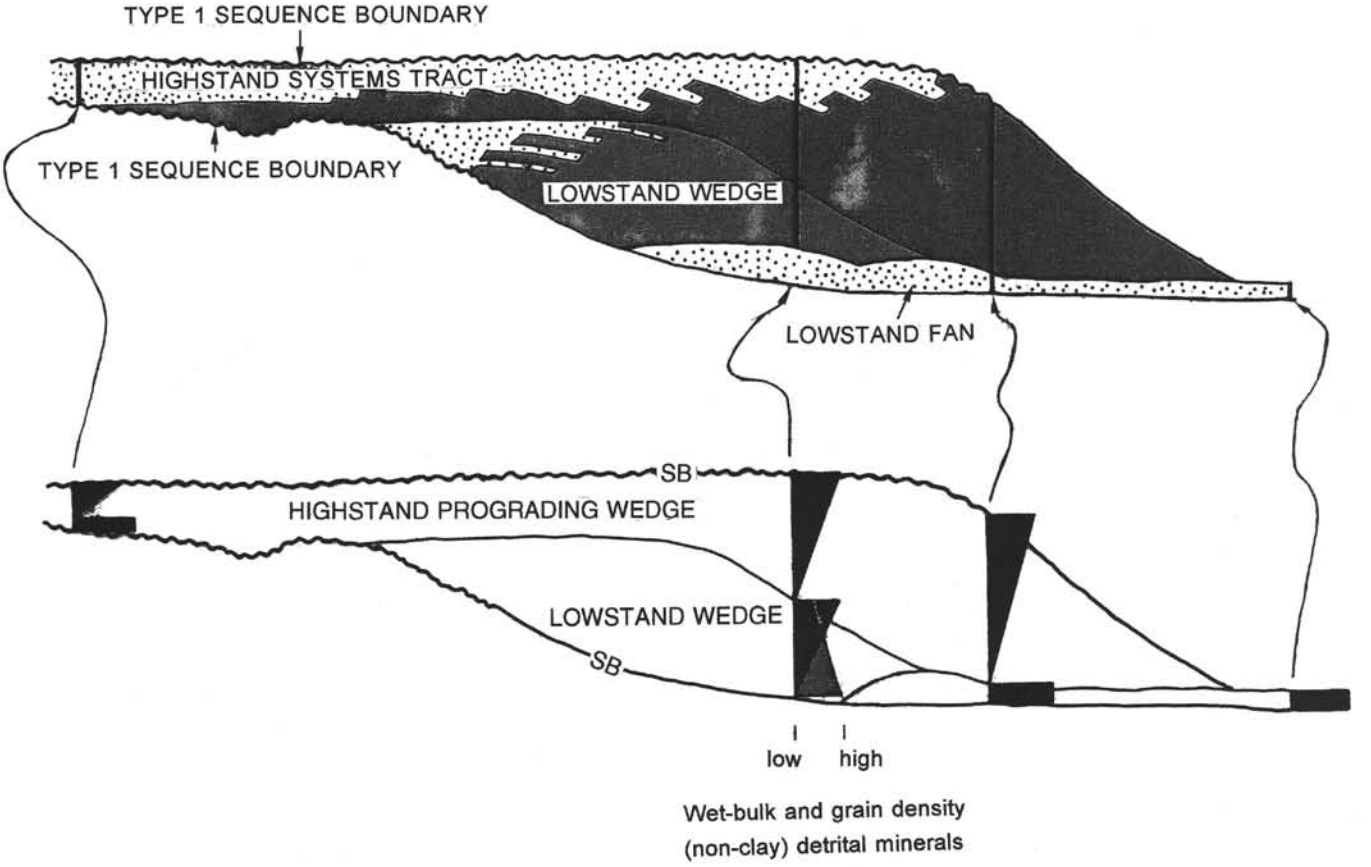

Figure 10. Synthetic interpretation of the sequence stratigraphic position of the Miocene intervals at Site 903 and onshore boreholes of the New Jersey transect compared with the Greenlee et al. (1992) sequence model for the New Jersey Margin. Thin intervals with characteristic lithology (symbolized by black rectangles) reflect deposition in lowstand fans (mainly below the main sequence body). Intervals with low, cyclically upward-increasing properties occur in prograding lowstand and highstand wedges (black triangles). In the Miocene, one such lowstand or highstand wedge prograded over a lowstand fan. In sequences where a highstand wedge follows a lowstand wedge, however, the latter shows a more complex trend with slightly upward decreasing properties (gray triangle). Properties of onshore borehole sequences, composed of basal glauconitic sand overlain by mud which increases upward in sand content (K.G. Miller, pers. comm., 1994), are inferred in analogy to such sediments at Site 903. There is no recognizable transgressive systems tract in this type of sequence, deposited under high sediment input/accommodation space ratios.

Table 3. Depositional sequences, systems tracts, and their boundaries based on interpretations of seismic geometries and upcore changes in interval characteristics.

Boundary codes		Boundary geometry	Interval code	Parameter trends	Systems tract	Bounding surface
m1.5	orange	Unconformity				SB
(—)		?Conformity	1	Low, increasing	LST/HST wedge	TS
m2	yellow2	Unconformity	2	High, ±constant	LST fan	SB
(—)		?Conformity	3	Low, increasing	HST wedge	TS
m3	blue	Unconformity	4	High, decreasing	LST wedge	SB
m4	pink2	Unconformity	5	Low, increasing	LST/HST wedge	SB
m5	green	Unconformity	6	High, ±constant	LST fan	SB
m5.4	sand	Conformity	7	Low, increasing	HST wedge	TS
m6	pink3	Unconformity	8	Low, decreasing	LST wedge	SB
(—)		?Conformity	9	High, ±constant	(dss)	?
o1	green3	Unconformity	10	High, ±constant	(dss)	SB

Notes: LST = lowstand systems tract, HST = highstand systems tract, SB = sequence boundary, TS = transgressive surface or top of lowstand systems tract surface, and (dss) = distal slope sediments (no systems tract specified). Boundary codes from Shipboard Scientific Party (1994a) and Greenlee et al. (1992); boundary geometries from Mountain, Miller, et al. (this volume).